Scale-Dependent Friction-Coverage Relations and Non-Local Dissipation in Surfactant Monolayers

Hongyu Gao,[†,§] James P. Ewen,[‡,§] Remco Hartkamp,[¶] Martin H. Müser,[†] and Daniele Dini[*,‡]

†*Department of Materials Science and Engineering, Universität des Saarlandes, 66123 Saarbrücken, Germany*

‡*Department of Mechanical Engineering, Imperial College London, London SW7 2AZ, UK*

¶*Process and Energy Department, Delft University of Technology, Leeghwaterstraat 39, 2628 CB Delft, The Netherlands*

§*H.G. and J.P.E. contributed equally*

E-mail: j.ewen@imperial.ac.uk

Abstract

Surfactant molecules, known as organic friction modifiers (OFMs), are added to lubricants to reduce friction and wear between sliding surfaces. In macroscale experiments, friction generally decreases as the coverage of OFM molecules on the sliding surfaces increases. However, recent nanoscale experiments with sharp atomic force microscopy (AFM) tips have shown increasing friction. To elucidate the origin of these opposite trends, we use nonequilibrium molecular dynamics (NEMD) simulations and study kinetic friction between OFM monolayers and an indenting nanoscale asperity. For this purpose, we study various coverages of stearamide OFMs on iron oxide surfaces and silica AFM tips with different radii of curvature. For our small tip radii, the friction coefficient and indentation depth both have a non-monotonic dependence on OFM

surface coverage, with maxima occurring at intermediate coverage. This suggests that friction is dominated by plowing. We rationalise the non-monotonic relations through a competition of two effects (confinement and packing density) that varying the surface coverage has on the effective stiffness of the OFM monolayers. We also show that kinetic friction is not very sensitive to the sliding velocity in the range studied, indicating that it originates from instabilities. Indeed, while friction predominately originates from the plowing action of the monolayers by the leading edge of the tip, thermal dissipation is mostly localised in molecules towards the trailing edge of the tip.

Introduction

Nanometer-thick surfactant films absorbed on solid surfaces are important to the effective operation of many engineering systems. In particular, such films are critical to mitigate against generally deleterious phenomena such as friction,[1] corrosion,[2] and agglomeration.[3] Organic friction modifiers (OFMs) are amphiphilic surfactants that are added to lubricants to reduce friction and wear between sliding surfaces.[4] Carboxylic acid, amine, amide, or ester surfactants with alkyl tailgroups containing between 12-20 carbon atoms are usually used for this purpose. OFMs are particularly important in the boundary lubrication regime, where the load is primarily supported by contacting solid asperities rather than the liquid lubricant. The boundary regime occurs in components that operate at low sliding velocity, v_{s}, and high pressure, P, or when lubricants with low viscosity, η, are used. Over the last few decades, lubricant viscosity has been progressively reduced to minimise hydrodynamic friction losses. This means that a greater number of lubricated machine components operate under boundary lubrication conditions, making additives that reduce friction and wear in this regime increasingly important to improve energy efficiency and ensure reliable operation.[5]

To rationally design improved OFM molecules, a detailed understanding of the atomic-scale behaviour governing their macroscale tribological performance is required. However, the physicochemical mechanisms leading to the reduction of friction and wear by OFMs have

been debated for almost a century. Much of the uncertainty originates from the fact that the films formed by OFMs are extremely thin ($\approx$ 2 nm) and fragile when extracted from the liquid phase.[4] In 1922, Hardy and Doubleday[6] showed that carboxylic acids produced a progressively lower friction on both glass and steel surfaces as their alkyl chain length was increased from C_4 to C_{12}. They postulated that the reduction in friction was due to the formation of vertically-oriented surfactant monolayers on the sliding surfaces.[6] Bowden and Leben[7] compared the friction of steel surfaces lubricated by stearic acid (C_{18}) deposited using the Langmuir-Blodgett technique[8] and the same carboxylic acid dissolved in a nonpolar base oil. They showed that a single monolayer of stearic acid was initially able to reduce friction down to the same level as that produced by the steel surfaces immersed in stearic acid dissolved in the base oil.[7] These close-packed monolayer films formed from solution would today be referred to as self-assembled monolayers (SAMs).[9] Several macroscale tribometer studies have shown that, as OFM concentration in a nonpolar base oil is increased, friction decreases before reaching a minimum value.[10–12] This minimum friction is generally attributed to the formation of a close-packed monolayer, with complete surface coverage.[4] However, in a recent study, Jaishankar et al.[13] have suggested that minimum friction occurs at much lower OFM surface coverages.

The first *in situ* observation of monolayer OFM films was not until 1996, when Spikes[14] applied ultrathin film interferometry inside a steel/steel contact lubricated by stearic acid dissolved in a nonpolar base oil. Over the last few decades, OFM monolayers have been observed on a range of surfaces using techniques including the quartz crystal microbalance (QCM)[13,15–17] and polarized neutron reflectometry (PNR).[18,19] While QCM and PNR can be used to investigate the thickness and surface coverage of OFM monolayers at solid-liquid interfaces, they cannot be applied inside rubbing contacts. On the other hand, *in situ* atomic force microscopy (AFM) can simultaneously probe the structure and friction of thin films at solid-liquid interfaces.[1,20] Indeed, AFM experiments have been used to study the film structure[21–23] and friction[16,24] of the monolayers formed by a range of OFMs on solid

surfaces from base oil solution.

Recently, two experimental studies have given important insights regarding the relationship between OFM surface coverage and friction. Fry et al.[17] studied the effect of surface coverage and friction for several OFMs with different headgroups and tailgroups in macroscale tribology experiments. They showed using QCM and spectroscopic ellipsometry that OFMs that formed monolayers with lower surface coverage gave higher initial friction coefficients.[17] The same trend was observed at the nanoscale for a wide range of SAMs using AFM tips with a relatively large radius of curvature, $r_{\mathrm{tip}} \approx 50$ nm.[25–33] Similar friction-coverage behaviour was also observed at the microscale for aromatic thiol SAMs on silver surfaces using the surface force apparatus (SFA).[34] However, recent AFM experiments by Nalam et al.[16] using sharper AFM tips ($r_{\mathrm{tip}} \approx 15$ nm) showed the opposite trend, i.e. the friction coefficient increased with increasing OFM surface coverage. The authors attributed this observation to faster rates of adsorption for the OFMs that form lower coverage films.[16]

Molecular dynamics (MD) simulations can also provide atomic-level insights into the structure and friction behaviour of OFM films in tribological contacts.[35] For example, NEMD simulations have been used to study a range of OFMs (carboxylic acids, amides, esters) with C_{18} tailgroups adsorbed on atomically-smooth α-Fe_2O_3 surfaces[36,37] and α-Fe with nanoscale roughness features.[38,39] In these studies, OFM monolayers with higher surface coverage ($\Gamma = 4.3$ nm^{-2}) generally showed lower friction ($\Gamma = 1.4$ nm^{-2}).[37] This rationalised the higher friction observed in macroscale tribology experiments for OFMs with Z-unsaturated tailgroups (e.g. oleic acid) compared to those with saturated tailgroups (e.g. stearic acid),[40] which have been shown to form monolayers with lower surface coverage in PNR experiments.[19]

Several MD simulations have also been performed to study the compression of other types of SAMs by single nanoscale asperities. For example, Tutein et al.[41] indented close-packed monolayers ($\Gamma = 4.5$ nm^{-2}) of linear alkyl chains (C_8, C_{13}, and C_{22}) chemically bound to a diamond (111) substrate with a capped carbon nanotube tip ($r_{\mathrm{tip}} < 1$ nm). During compression, the number of gauche defects within the chains increased underneath the tip.[41] This

observation was experimentally confirmed using AFM experiments of Langmuir-Blodgett films and SAMs of octadecyltrichlorosilane (OTS) on quartz, mica, and gold surfaces.[42] In another MD study, Meltzer et al.[43] used a repulsive sphere ($r_{\mathrm{tip}} = 3$ nm) to compress high coverage ($\Gamma = 3.8$–5.1 nm^{-2}) octadecylphosphonic acid (ODPA) monolayers adsorbed on α-$Al_2O_3(0001)$. They observed a spatial anisotropy of pressure-induced defects within ODPA domains; molecules whose initial tilt was in the direction of the pressure gradient increased in tilt angle, while those tilted away formed gauche-defects.[43] Ewers and Batteas[44,45] investigated the compression of OTS films adsorbed on amorphous silica (a-SiO_2) surfaces at a range of coverages ($\Gamma = 1.5$–3.5 nm^{-2}) with a hemispherical a-SiO_2 tip ($r_{\mathrm{tip}} = 4.5$ nm). As the surface coverage was increased, a sharp transition was observed from the narrow, high-pressure interaction between the underlying substrates, to a broad, substantially lower pressure interaction.[44,45]

Some NEMD simulations have also been performed to study the frictional response of SAMs penetrated by single nanoscale asperities. For example, Knippenberg et al.[46] studied friction in a close-packed ($\Gamma = 4.6$ nm^{-2}) alkyl monolayer (C_{14}) indented with a spherical fullerene tip ($r_{\mathrm{tip}} = 1.3$ nm) at high sliding velocity ($v_{\mathrm{s}} = 87$ m s^{-1}). In agreement with previous experiments for OTS on a-SiO_2 surfaces,[32] they showed that plowing of adsorbed monolayers can be a significant contribution to friction.[46] Chandross et al.[47] studied the indentation and friction of close-packed ($\Gamma = 4.0$ nm^{-2}) alkylsilane molecules (C_8-C_{18}) adsorbed on a-SiO_2 substrates with hemispherical a-SiO_2 tips ($r_{\mathrm{tip}} = 3$–30 nm) at $v_{\mathrm{s}} = 2$ m s^{-1}. They found that, although the friction force, F_{F}, increased when the tip radius was increased due to adhesion, the friction coefficient, μ, was almost independent of the tip radius.[47] In a recent study, Summers et al.[48] also studied friction in alkylsilane molecules (C_{18}) adsorbed at different Γ (2.0-5.0 nm^{-2}) on a-SiO_2 substrates indented by hemispherical and flat a-SiO_2 AFM tips ($r_{\mathrm{tip}} = 2$ nm) at $v_{\mathrm{s}} = 10$ m s^{-1}. For the hemispherical tip, they found that μ increased with increasing Γ,[48] as observed experimentally by Nalam et al.[16]

In this study, we use NEMD simulations to investigate frictional dissipation in stearamide

(C_{18}) OFM films adsorbed on an atomically-smooth α-Fe_2O_3 surface indented by an a-SiO_2 tip. An accurate all-atom force field[49,50] with OFM-surface interactions optimized from density functional theory (DFT) calculations[51,52] is employed. The effects of tip radius (r_{tip} = 3–12 nm), sliding velocity (v_s = 2–50 m s^{-1}), and surface coverage (Γ = 2–5 nm^{-2}) on the nanoscale structure and friction of the amide monolayers are investigated. The results provide insight into the frictional response of monolayer OFM films adsorbed on solid surfaces and indented by sliding nanoscale asperities.

Methodology

Simulation setup

The investigated systems consist of an a-SiO_2 tip above an atomically-smooth hematite (α-Fe_2O_3) substrate that is covered by an amide OFM monolayer, as shown in Fig. 1a. The setup closely matches that used by Nalam et al.[16] for their AFM experiments. Most of the tips used in AFM experiments are made from Si or Si_3N_4,[47] which will quickly oxidise when exposed to air to form an outer SiO_2 layer.[53] In AFM experiments, Si-based tip radii are generally of the order of tens of nanometers.[47] In this study, a-SiO_2 tips with two different sizes, (r_{tip} = 4–12 nm) are used, which are similar to those employed in previous experimental[16] and NEMD studies.[47,48] A hemicylindrical tip shape is employed, which is periodic in the y-direction.[54] Compared to a hemispherical tips, hemicylindrical tips decouple the required system size in the y-direction from the other directions, which can drastically reduce the computational expense for large tip radii.[55] The α-Fe_2O_3 substrate is used as a model for steel surfaces, which form outer oxide layers when exposed to air.[56] The α-Fe_2O_3(0001) surface is chosen because of its high thermodynamic stability.[51] The substrate is periodic in the x and y directions and has dimensions of: x = 20.2 nm, y = 2.8 nm, and z = 1.5 nm. 10 nm of space was added above the substrate in the z-direction.

Stearamide ($C_{18}H_{37}NO$), a surfactant with an amide headgroup and a saturated linear

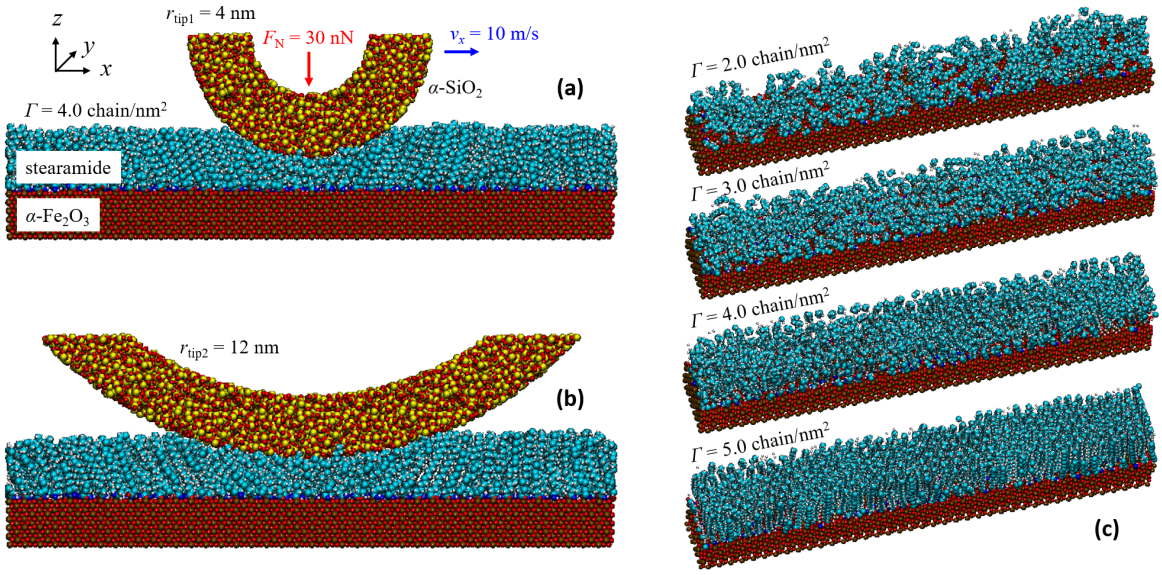

Figure 1: Snapshots of representative systems of stearamide monolayers ($\Gamma = 4$ nm^{-2}) on α-Fe_2O_3 substrates ($x = 20.2$ nm, $y = 2.8$ nm, and $z = 1.5$ nm) indented by a-SiO_2 tips, with $r_{tip} = 4$ nm (a) and 12 nm (b). Snapshots of stearamide monolayers with surface coverage (c), $\Gamma = 2$–5 nm^{-2} on α-Fe_2O_3 (tips not shown). Rendered with VMD:[57] Fe atoms are shown in brown, O in red, N in blue, C in cyan, H in white, and Si in yellow.

C_{18} tailgroup, was chosen as a model OFM.[4] In addition to their use as OFM additives in engine lubricants for steel surfaces, fatty amides are also used to control friction in automatic transmission fluids,[58] and for polymer processing.[59,60] Stearamide monolayers were preformed at different surface coverage, similar to the films formed using the Langmuir-Blodgett method.[8] Four different coverages (Γ = 2–5 nm^{-2}) are considered, with stearamide molecules randomly distributed on the α-Fe_2O_2(0001) substrate, as shown in Fig. 1b. These are the same coverages considered by Summers et al.[48] in their NEMD simulations of OTS monolayers on a-SiO_2 surfaces. The concentration of OFMs in a base oil, rather than the surface coverage, is typically varied in macroscale tribology experiments,[40] since this is much easier to measure and control. However, depletion isotherm, PNR,[18,19] and QCM experiments[13,15–17] can be used to measure the surface coverage at a given OFM concentration. Adsorption experiments have not been performed for stearamide OFMs on iron oxide surfaces, but such experiments for stearic acid suggested a maximum $\Gamma \approx 4$ nm^{-2} on iron oxide from n-dodecane.[19] To minimise the computational expense, nonpolar base oil molecules are not considered in this study. This is not expected to significantly affect the friction results, which are supposedly dominated by plowing of the adsorbed monolayers.[32,46]

Force field

The stearamide molecules are represented with the Long chain-Optimized Potential for Liquid Simulations-All Atom (L-OPLS-AA) force field.[49,50] This force field has been shown to accurately describe the structure and friction behaviour of OFM monolayers adsorbed on iron oxide surfaces.[61] The bonded and unbonded parameters of the stearamide molecule can be found in Ref. 49 (N, O) and Ref. 50 (C, H).

In the α-Fe_2O_3 substrate, harmonic bonds with a force constant of 130 kcal mol^{-1} Å^{-1} were added between atoms within 0.3 nm of each other in their lattice positions. The bond lengths were based on the interatomic distances reported by Blake et al.[62] from diffraction experiments. This has been shown in previous simulations to provide both realistic

mechanical properties and efficient thermal dissipation.[63] DFT calculations of hexanamide adsorption on α-Fe_2O_3(0001) have shown strong chemisorption interactions to occur between amide headgroups and the surface atoms.[51] For the force field used in this study, the molecule-surface parameters were optimised to match DFT adsorption energies for a wide range of conformations of amides on α-Fe_2O_3(0001).[52] Morse and Coulomb potentials were used for the strong headgroup-surface interactions (O_{amide}-Fe_{surf}, N_{amide}-Fe_{surf}, H_{amide}-O_{surf}), while Lennard-Jones and Coulomb potentials were used for the weaker tailgroup-surface interactions.[52] The headgroup-surface Morse parameters, as well as Fe and O Lennard-Jones and partial charge parameters, are given in Ref. 52.

The a-SiO_2 tip was prepared by annealing β-cristobalite using a modified van Beest-Kramer-van Santen potential.[64] The β-cristobalite cell was heated to 4,000 K and quenched to 300 K at a cooling rate of 2.5 K ps^{-1}, which yielded a-SiO_2 with a density of 2.2 g cm^{-3}. The full procedure for the annealing is described in Ref. 65. From this system, hemicylinders were cleaved, which were then energy minimised using the same potential. In the indentation and sliding simulations, the tips were treated as rigid bodies, as in previous NEMD studies.[48] The Si and O Lennard-Jones and partial charge parameters for atoms in the tips, which control the tip-amide and tip-substrate interactions, were taken from Ref. 48.

Geometric mean mixing rules were used for Lennard-Jones interactions between unlike atoms.[49] The Lennard-Jones and Morse interactions were cut off at a distance of 1.2 nm.[52] A slab implementation of the particle-particle, particle-mesh algorithm[66] with a relative force accuracy of 10^{-5} was used for the Coulombic interactions.

Simulation procedure

NEMD simulations were performed using the Large-scale Atomic/Molecular Massively Parallel Simulator (LAMMPS) software.[67] The velocity Verlet integration algorithm was used with a time step of 1 fs. First, the systems were energy minimised before they were equilibrated at a temperature of 300 K for 1 ns. The positions of the bottom layer of atoms (0

nm $< z <$ 0.1 nm) in the α-Fe_2O_3(0001) substrate were fixed. Temperature was controlled with a Langevin thermostat with a coupling time of 0.1 ps.[68] The thermostat was applied to the middle layer (0.1 nm $< z <$ 1.0 nm) of substrate atoms and was coupled to the thermal velocities in the direction perpendicular to both compression and sliding (y). Several previous studies have demonstrated the importance of thermostatting the substrate rather than the fluid molecules during confined NEMD simulations.[69–71]

After the system was equilibrated, a constant normal force (1–30 nN) was added to the tip in the z-direction to compress the stearamide monolayer. Similar loads have been used in previous MD simulation studies of monolayers indentation by nanoscale asperities.[46–48] These forces lead to estimated mean Hertz pressures, P_{mean} = 0.04–2 GPa for the tip sizes considered (r_{tip} = 4–12 nm). These P values are directly relevant to AFM experiments of OFM films[16] as well as the operation of OFMs under boundary lubrication conditions.[4] Compression simulations were performed for approximately 1 ns, which was the time taken for the tip-surface distance and average normal force on the tip to reach a steady state.

Next, the tip was moved at a constant sliding velocity, v_{s}, in the x-direction. In most NEMD simulations of the current study, v_{s} = 10 m s^{-1}, but other values (v_{s} = 2–50 m s^{-1}) were also considered in a subset of simulations. Similar v_{s} values have been applied in previous NEMD simulations of monolayers indented by nanoscale asperities.[46–48] The NEMD velocities are several orders of magnitude higher than those reached in AFM experiments ($\mathcal{O}$ μm s^{-1})[28,29,32,33] or macroscale tribology experiments ($\mathcal{O}$ mm s^{-1}).[17,40] The sliding velocities are, however, quite similar ($\mathcal{O}$ m s^{-1}) to those which are experienced by components in applications such as micro-electromechanical systems[72] and internal combustion engines.[73] The normal and friction forces represent the total forces on the sliding tip in response to the monolayer in the z and x directions respectively. The sliding simulations were performed for sufficient sliding distance (50 nm) to ensure that a nonequilibrium steady state was obtained for all v_{s} values considered.[74] For v_{s} = 10 m s^{-1}, this required sliding simulations to be run for 5 ns. The normal and friction forces presented in the Results and Discussion section were

averaged over the final 30 nm of sliding (3 ns at 10 m s^{-1}). Previous NEMD simulations have shown that friction asymmetry can be significant for alkylthiol monolayers adsorbed on flat Au(111) substrates.[75] In these simulations, the friction force was dependent on the direction of sliding relative to the molecular tilt direction.[75] However, for the nanoscale asperity systems studied in the current simulations, friction asymmetry was negligible.

Results and Discussion

Indentation Depth

In order to understand the frictional dissipation within the OFM monolayers, we first investigated the indentation depth of the tip during sliding for the different systems and conditions considered. Fig. 2 shows how the monolayer film thickness, h, varies along the sliding direction (x), with a lateral resolution of 0.5 nm for $r_{\mathrm{tip}} = 4$ nm (a) and 12 nm (b). Here, h is defined as the distance between the centre of the topmost substrate atoms and the topmost stearamide atoms in the z-direction. The x-coordinates in Fig. 2 are relative to the centre of the tip.

In Fig. 2, a reduction in film thickness is observed underneath the tip centre in all cases, indicating indentation of the stearamide monolayers during sliding. This suggests that thickness is reduced either due to viscoelastic deformation[76] or plowing[32,46] of the monolayers by the tip. The average monolayer film thickness in the z-direction can be determined from the height of the monolayer in the undisturbed region of the film thickness profiles (away from the tip centre). The lateral dimensions are sufficiently large such that, in the undisturbed region, h is the same as in the absence of the tip within statistical uncertainty. In the undisturbed region, h increases with increasing coverage, from 1.2 nm at $\Gamma = 2$ nm^{-2} to 2.3 nm at $\Gamma = 5$ nm^{-2}. These values are within 5 % of those obtained in previous simulations of OTS (also linear, C_{18} tailgroup) monolayers on a-SiO_2 surfaces.[48]

The h profiles in Fig. 2 are mostly symmetrical, with tailgroups underneath the tip being

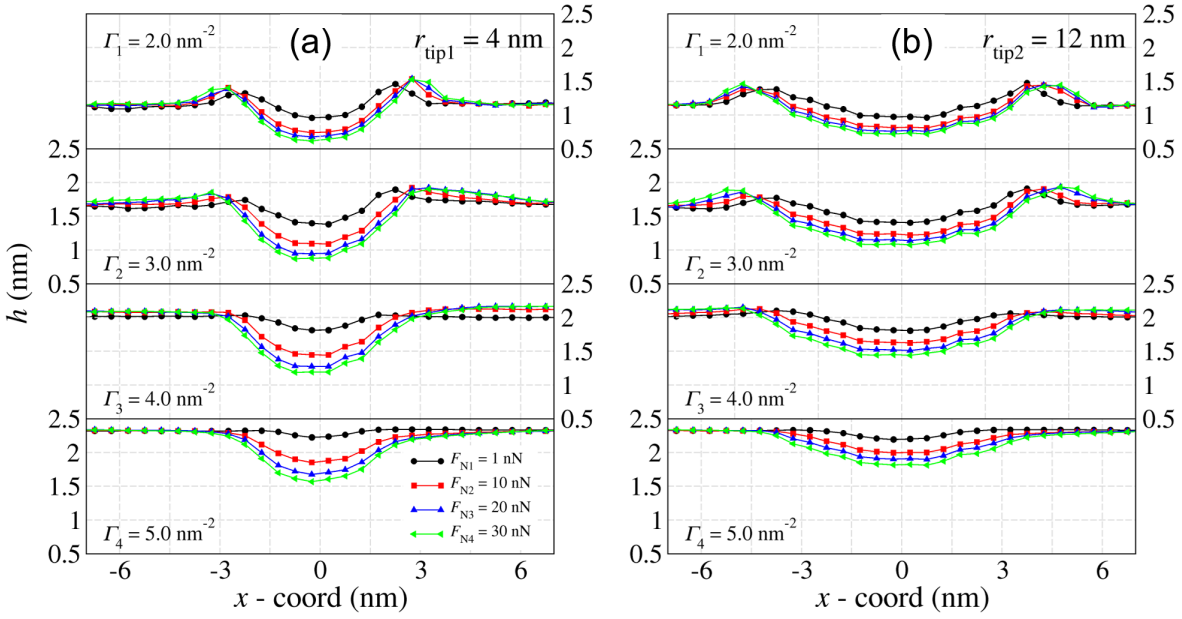

Figure 2: Film thickness, h, profiles in the sliding direction (x) for tip radius, $r_{\mathrm{tip}} = 4$ nm (a) and $r_{\mathrm{tip}} = 12$ nm (b). Coordinates are relative to the tip centre.

compressed and displaced towards the leading and trailing edges of the tip. As expected, the sharper tip (Fig. 2a) shows deeper, more localised penetration than the blunter tip (Fig. 2b). An increase in h compared to the undisturbed region at the leading (pileup) and trailing (debris) edge of the tip is observed at low coverage (Γ = 2–3 nm^{-2}). Similar behaviour has previously been observed in indentation NEMD simulations of solid iron[77] and OTS monolayers on a-SiO_2 surfaces.[48] At high coverage (Γ = 5 nm^{-2}), there is a small reduction in h (depletion) at the leading edge of the tip. This is due to the closely-packed molecules being pulled downwards to accommodate tip motion over neighbouring molecules, even before they come into direct contact with the tip. Even for the lowest coverage (Γ = 2 nm^{-2}), smallest tip ($r_{\mathrm{tip}} = 4$ nm), and largest load ($F_{\mathrm{N}} = 30$ nN) considered, the tip and the substrate remain separated at a distance of approximately 0.5 nm. Moreover, AFM experiments of hexadecanethiol monolayers on the Au(111) surface suggested that they were durable up to an average pressure of 3.7 GPa.[78] These observations suggest that OFMs should usually prevent direct solid-solid contact under very high pressures ($>$ 2 GPa), even

at relatively low surface coverage.[13]

Fig. 3 shows the change in tip-monolayer indentation depth, d_p, with surface coverage, Γ, for the different loads, F_{N}, considered. Here, d_p is defined as the difference between the z-positions of the bottom of the tip and the top of the amide monolayer. For all of the systems studied, $d_p > 0.1$ nm, and d_p increases with increasing load. This suggests that plowing of the monolayers by the tip will represent a significant contribution to friction,[32,46] even for the lowest load (1 nN) considered.

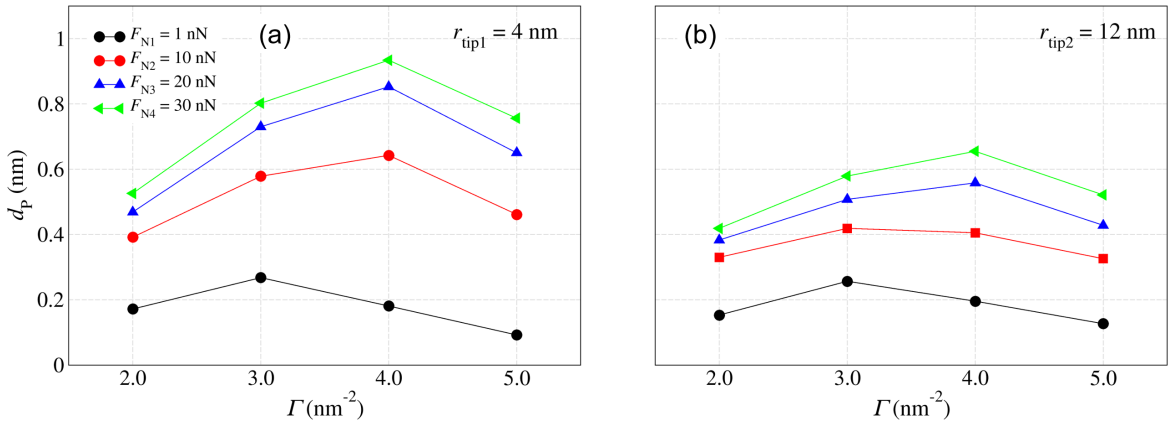

Figure 3: Change in tip-monolayer indentation depth, d_p, with surface coverage, Γ, for the different loads, F_{N}, considered with $r_{\mathrm{tip}} = 4$ nm (a) and $r_{\mathrm{tip}} = 12$ nm (b).

A deeper indentation is revealed $r_{\mathrm{tip}} = 4$ nm (Fig. 3a) compared to $r_{\mathrm{tip}} = 12$ nm (Fig. 3b), which is due to the reduced contact area and thus higher pressure. For both tip sizes, d_p increases markedly with load between $F_{\mathrm{N}} = 1$–10 nN, to a lesser degree between 10–20 nN, and remains almost constant between 20–30 nN. This suggests that collective molecular tilt and molecular defects[42] can accommodate the indentation of the tip only up to a certain point, beyond which the monolayers become essentially incompressible. Since this occurs both at low coverage (where the tip-substrate distance is < 1 nm) and at high coverage (where the tip-substrate distance is > 1.5 nm), this observation is not purely attributable to confinement effects, as is the case for nonpolar fluids.[79] In Fig. 3, d_p has a non-monotonic dependence on surface coverage, with the maximum indentation depth occurring at intermediate coverage

(usually $\Gamma = 4$ nm^{-2}). This suggests that the elastic modulus of the films increases between $\Gamma = 2$–4 nm^{-2} and then decreases between $\Gamma = 4$–5 nm^{-2}. As Γ is increased, there are two competing effects which determine the elastic moduli of the monolayers; i) decreasing confinement-induced viscosity enhancement and ii) increasing headgroup packing density. While between $\Gamma = 2$–4 nm^{-2}, the decrease in (i) is outweighed by the increase in (ii), the opposite is true between $\Gamma = 4$–5 nm^{-2}. Interestingly, the h at which this transition occurs (> 2 nm in Fig. 2) coincides with the distance at which confinement-induced viscosity enhancement become negligible for alkane molecules confined between solid surfaces.[80] Thus, despite the OFM molecules being more densely packed at $\Gamma = 5$ nm^{-2} than at $\Gamma = 4$ nm^{-2}, the monolayers are more compliant due to the absence of confinement effects.

Friction

We also investigated the kinetic friction within the indented monolayers during sliding of the tips. Fig. 4 shows the change in the friction force, F_{F}, with normal force, F_{N}, for the different Γ and r_{tip} values considered.

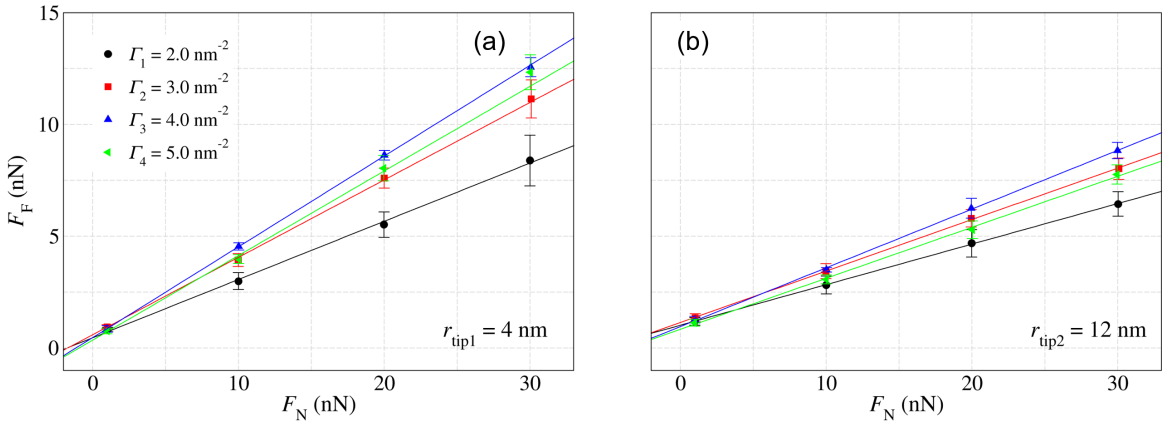

Figure 4: Change in the friction force, F_{F}, with normal force, F_{N}, for the different surface coverages, Γ, of stearamide considered (2–5 nm^{-2}) with a 4 nm (a) and 12 nm (b) tip radius, r_{tip}. Solid lines are linear fits to the data. Error bars represent one standard deviation between the block-averaged values.

For both tip sizes, F_{F} increases linearly with F_{N} with a finite intercept in Fig. 4. This linear trend is consistent with Amontons' first law of friction, $F_{\mathrm{F}} = \mu F_{\mathrm{N}}$, where μ is the coefficient of friction. Since this expression cannot account for the non-zero intercepts observed in Fig. 4, Derjaguin[81] proposed a modification:

$$F_{\mathrm{F}} = \mu F_{\mathrm{N}} + F_0 \tag{1}$$

where F_0 is the so-called Derjaguin offset which is attributable to adhesive forces. This expression was used by Briscoe and Evans[82] to describe the friction between Langmuir-Blodgett[8] films of carboxylic acid OFMs (C_{14}-C_{22}) on atomically-smooth mica substrates. The expression has frequently been used to describe friction data from AFM experiments of SAMs on solid surfaces[30,83] as well as NEMD simulations of OFM monolayers on surfaces with nanoscale roughness features.[38,39] Expressions which separate the frictional contribution due to plowing of SAMs have been proposed by Brukman et al.[31] and Flater et al.[32] to describe AFM data. Such expressions are only required when the F_{F} versus F_{N} plot is non-linear, which is not the case for any of the systems in Fig. 4. Therefore, we use the simpler modified form of Amontons' first law of friction due to Derjaguin[81] to describe our F_{F} versus F_{N} data, see Equation (1).

Comparing Fig. 4a and Fig. 4b, F_{F} is higher for the 4 nm tip than for the 12 nm tip at all but the lowest normal force considered. For both tip sizes, the gradient of the increase in F_{F} with F_{N} is generally steeper at high Γ than at low Γ. This is in agreement with previous NEMD simulations of OTS monolayers on a-SiO_2 surfaces indented by a sharp hemispherical a-SiO_2 tip ($r_{\mathrm{tip}} = 2$ nm) by Summers et al.[48] For all Γ values considered, F_{F} increases with a shallower gradient for $r_{\mathrm{tip}} = 12$ nm than for $r_{\mathrm{tip}} = 4$ nm. The gradients and intercepts of the linear fits in Fig. 4 were used to calculate μ and F_0, respectively, using Equation (1).[81]

Fig. 5 shows the change in coefficient of friction, μ (a) and Derjaguin offset, F_0 (b) with Γ for the two r_{tip} values considered. It is clear from Fig. 5a that, for all of the Γ values considered, μ is higher for $r_{\mathrm{tip}} = 4$ nm than for $r_{\mathrm{tip}} = 12$ nm. The larger μ for the smaller

tip is likely due to the larger pressure, which leads to deeper indentation (Fig. 3), and thus a larger plowing contribution to friction.[32,46] This observation is in contrast to previous NEMD simulations by Chandross et al.[47] that suggested μ was essentially independent of r_{tip} in the range 3–30 nm. These previous simulations used shorter alkyl tailgroups (C_{11}) and fewer F_{N} values spanning a narrower range (0–20 nN) to estimate μ than the current study.

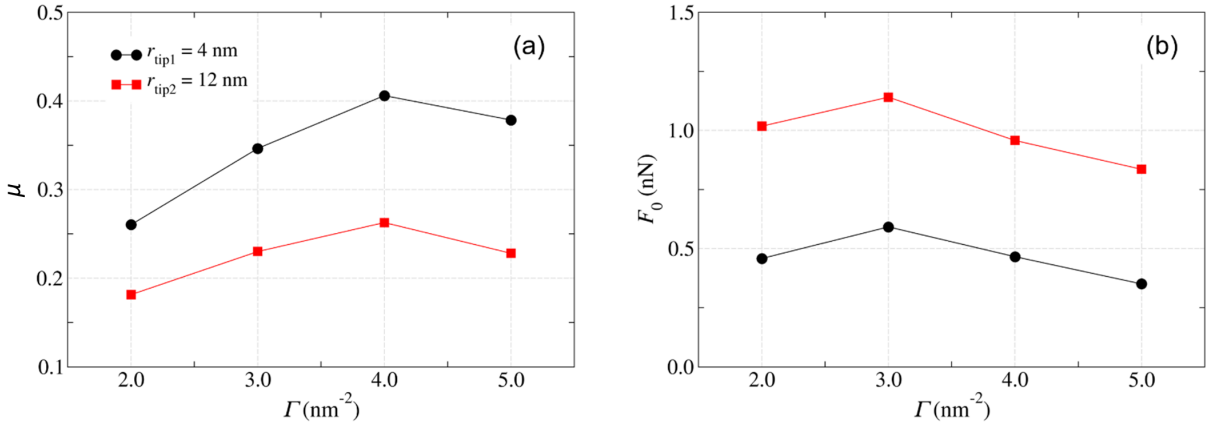

Figure 5: Change in the coefficient of friction, μ, (a) and Derjaguin offset, F_0, (b) with stearamide surface coverage, Γ, for tip radii, r_{tip} = 4 nm and 12 nm. Solid lines are guides for the eye.

Previous NEMD simulations of the same system with flat top and bottom surfaces, both coated with OFM molecules, gave μ values which decreased linearly from 0.22 at Γ = 1.4 nm^{-2} to 0.16 at Γ = 4.3 nm^{-2}.[52] The reduction in μ with increasing surface coverage is due to the formation of more solid-like monolayers, with reduced molecular interdigitation.[37,52] A reduction in μ with increasing Γ has recently been observed in macroscale tribology experiments by Fry et al.[17] They used OFM molecules with different headgroups and tailgroups to form monolayers with different surface coverages on silica surfaces.[17] The surface coverage, obtained using ellipsometry and QCM, was found to correlate with the initial friction coefficient, with minimum friction occurring at maximum coverage.[17]

The μ values in Fig. 5a with the top surface containing nanoscale curvature are larger (particularly for r_{tip} = 4 nm) than those from previous simulations with flat surfaces.[52] The same observation was made by Knippenberg et al.[84] from NEMD simulations comparing

friction from alkyl chains grafted on a diamond surface compressed by either a spherical fullerene tip or a flat amorphous carbon slab. Moreover, de Beer and Müser showed using NEMD that, for polymer brush-bearing surfaces, systems with nanoscale curvature provided additional dissipation mechanisms compared to those with flat surfaces.[85] In Fig. 5a, μ shows a non-monotonic dependence on surface coverage for both tip sizes, with the maximum friction coefficient occurring at intermediate coverage ($\Gamma = 4$ nm^{-2}). This coverage corresponds to the maximum indentation depth in Fig. 3, suggesting that the plowing contribution to μ increases with increasing d_p. Since d_p is load-dependent, it is challenging to separate the plowing contribution to μ using the expressions developed by Brukman et al.[31] and Flater et al.[32] for friction data from AFM experiments. Although it is beyond the scope of this current study, it should be possible to define a load-dependent term for the plowing contribution to μ. This could perhaps be achieved using geometrical considerations to estimate the indentation area from d_p, as proposed by Bowden and Tabor[86] to describe the friction of indented solids. However, this approach requires the assumption of isotropic hardness, which is unlikely hold for the SAM systems studied here.[79]

Non-monotonic friction-coverage behaviour has been observed experimentally at the microscale by Yoshizawa et al.[87] using the SFA. They employed zwitterionic surfactants with a range of headgroup and tailgroup structures to form monolayers with different coverages on mica surfaces in aqueous environments.[87] The non-monotonic response was attributed to a transition from liquid-like, to amorphous, and to solid-like monolayers with increasing coverage ($\Gamma = 2$–5 nm^{-2}).[87] However, despite a large number of AFM studies for a wide range of different SAMs,[25–33] non-monotonic friction-coverage behaviour has not been observed experimentally in non-aqueous environments. In these AFM experiments, surface coverage was varied in two main ways; i) changing the surfactant tailgroup length, ii) changing the surfactant headgroup. SAMs formed from surfactants with longer tailgroups (between C_3–C_{18}) are known to form more ordered films with higher surface coverage.[25–27] Moreover, surfactants with headgroups that interact more strongly with the surface, occupy a smaller

area, or contain multiple tailgroups, can all form SAMs with higher surface coverage.[28–33] All of these AFM studies showed a decrease in μ at higher Γ,[25–33] as was recently observed for OFM SAMs in macroscale tribology experiments.[17] These AFM studies used relatively blunt tips ($r_{\mathrm{tip}} \approx 50$ nm),[25–33] which, based on the results shown in Fig. 2 and Fig. 3, are likely to only give shallow indentation depths in the load range considered ($F_{\mathrm{N}} = 1$–30 nN). Conversely, Nalam et al.[16] used sharper AFM tips ($r_{\mathrm{tip}} \approx 15$ nm), and so similar indentation depths are expected to those shown from the current simulations in Fig. 3b ($r_{\mathrm{tip}} = 12$ nm). Nalam et al.[16] found that μ increased with increasing Γ for amine OFM monolayers on steel surfaces. Using NEMD simulations, Summers et al.[48] also showed that μ increased with increasing Γ for OTS SAMs indented by a very sharp AFM tip ($r_{\mathrm{tip}} = 3$ nm). Thus, previous experiments and simulations have both shown that monolayers with higher coverage can cause higher friction when sharp tips are used and friction is dominated by molecular plowing. In Fig. 5a, the same trend is observed between low and intermediate coverage (Γ 2–4 nm^{-2}). However, a decrease in μ between intermediate and high coverage (Γ 4–5 nm^{-2}) was observed, which was not seen in the experiments by Nalam et al.[16] Previous depletion isotherm and PNR experiments[19] suggest that the OFMs used by Nalam et al.,[16] which contained a mixture of saturated and Z-unsaturated tailgroups, were unlikely to have reached the highest coverage considered in the current study ($\Gamma = 5$ nm^{-2}). In future studies, we expect that non-monotonic friction-coverage behaviour will be observed experimentally using sharp AFM tips and surfactants known to form more closely-packed monolayers on solid surfaces (i.e. those with saturated tailgroups[19]).

All of the amide headgroups remain attached to the surface under even the most extreme conditions studied. This is due to the strong chemisorption interactions between the amide headgroup and surface atoms,[52] which were parameterised to reproduce interaction energies from accurate DFT calculations.[51] X-ray photoelectron spectroscopy experiments have shown that, like the fatty amides investigated in this study, fatty amines also chemisorb on steel surfaces,[18] and thus the monolayers are likely to show similar durability. From their

AFM and QCM experiments, Nalam et al.[16] postulated that the higher friction of fatty amine molecules which form higher coverage monolayers was due to their slower rate of adsorption. They suggested that the monolayers were damaged during sliding, and that slower healing led to higher friction.[16] For this to cause higher friction, a significant proportion of the adsorbed molecules would need to be removed from the surface during rubbing. The high durability of the fatty amide monolayers during the current simulations, and other SAMs in AFM experiments,[78] suggest that wear of the amine monolayers on steel surfaces is likely to be negligible under the conditions studied by Nalam et al.[16] Moreover, for friction to be controlled by differences in the rates of monolayer healing, the rate of adsorption would need to be comparable to the rubbing frequency. The adsorption rate constants obtained by Nalam et al.[16] from QCM varied between 0.012–0.001 s^{-1} for the different fatty amines studied, while AFM friction was essentially rubbing frequency-independent over a range spanning four decades (0.02–20 s^{-1}). If slower monolayer healing was the cause of higher friction, one would expect to see a significant increase in friction at higher scanning frequencies. Thus, the increase in friction for molecules forming monolayers with higher surface coverage observed by Nalam et al.[16] likely originates from differences in dissipation within the films, rather than rate of monolayer healing. In other words, in the experiments performed by Nalam et al.,[16] the higher friction at higher coverage can probably be attributed to deeper indentation depths (Fig. 3), causing a larger plowing contribution to friction.

Fig. 5b shows that adhesion, as quantified by F_0, is larger for the blunter tip, which is expected due to the larger tip-monolayer contact area. The same trend was also observed by Chandross et al.[47] in their NEMD simulations of alkylsilane monolayers. At very low load (F_N = 1 nN), F_0 can enhance F_F by more than 50 % in Fig. 5b. However, at higher loads, which are more application-relevant, F_0 becomes much less important (e.g. $<$ 10 % at 20 nN). In previous NEMD simulations of OFM monolayers with fully-periodic surfaces containing nanoscale roughness features, F_0 only significantly enhanced friction at low surface coverage.[38,39] In Fig. 5b, there is also a general decrease in F_0 with increasing surface coverage

for the single-asperity system studied here. From Fig. 2, this decrease in F_0 can be attributed to the general reduction in tip-monolayer contact area as surface coverage increases.

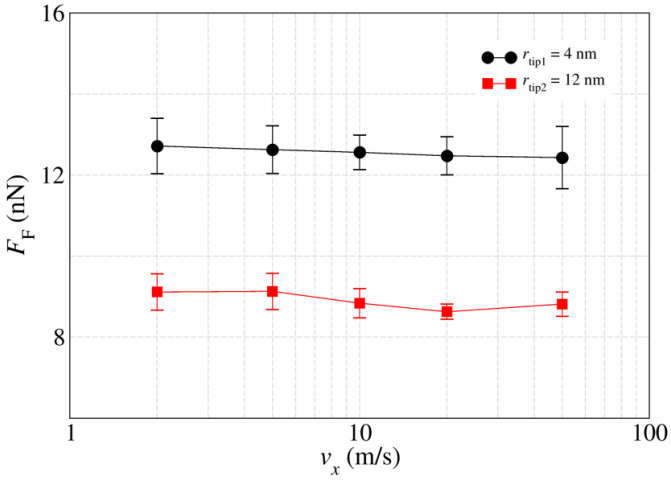

Figure 6: Change in the mean friction force, F_F, with sliding velocity v_s, with a surface coverage, $\Gamma = 4$ nm^{-2}, for tip radii, $r_{tip} = 4$ nm and 12 nm. Error bars represent one standard deviation. Solid lines are guides for the eye.

Fig. 6 shows the change in F_F with v_s with a high surface coverage ($\Gamma = 4$ nm^{-2}) for both tip sizes ($r_{tip} = 4$ nm and 12 nm). For both tip sizes, F_F is insensitive to sliding velocity in the range studied ($v_s = 2$–50 m s^{-1}). Previous simulations of OFM monolayers using flat surfaces have shown that μ increased logarithmically with v_s.[37] In macroscale tribology experiments, μ generally increases logarithmically with v_s for OFMs with saturated tailgroups (e.g stearic acid),[40] which form high Γ monolayers.[19] Microscale SFA experiments of Langmuir-Blodgett films of stearic acid also showed the same trend.[82] Conversely, for OFMs with Z-unsaturated tailgroups (e.g. oleic acid),[40] which form lower Γ monolayers,[19] μ was less sensitive to v_s. Nanoscale AFM experiments have generally shown that μ initially increases logarithmically with v_s before reaching a steady state value.[83,88] In the experiments performed by Nalam et al.,[16] μ was insensitive to v_s in the range studied (0.05–50 μm s^{-1}). Although v_s is several orders of magnitude higher in the NEMD simulations compared to the AFM experiments, efficient thermostatting ensures that the friction results are directly comparable, as shown

previously for OFM-lubricated systems.[37,61] The velocity-independence of the friction forces in the AFM experiments and NEMD simulations suggests an instability in the dissipation, as discussed in more detail below.

Fig. 7 shows the spatial distribution of the tip-monolayer shear stress, σ_{zx}, and normal stress, σ_{zz}, for both tip radii at the highest load considered ($F_{\mathrm{N}} = 30$ nN). The local stresses are calculated by dividing the sum of the tip-monolayer forces in each bin ($\Delta x = 0.2$ nm) by its area in the xy plane. The total stresses can be obtained by integrating over the area under these curves.[46] For σ_{zx}, positive values resist tip motion, while negative values assist tip motion. The x-coordinates in Fig. 7 are relative to the tip centre.

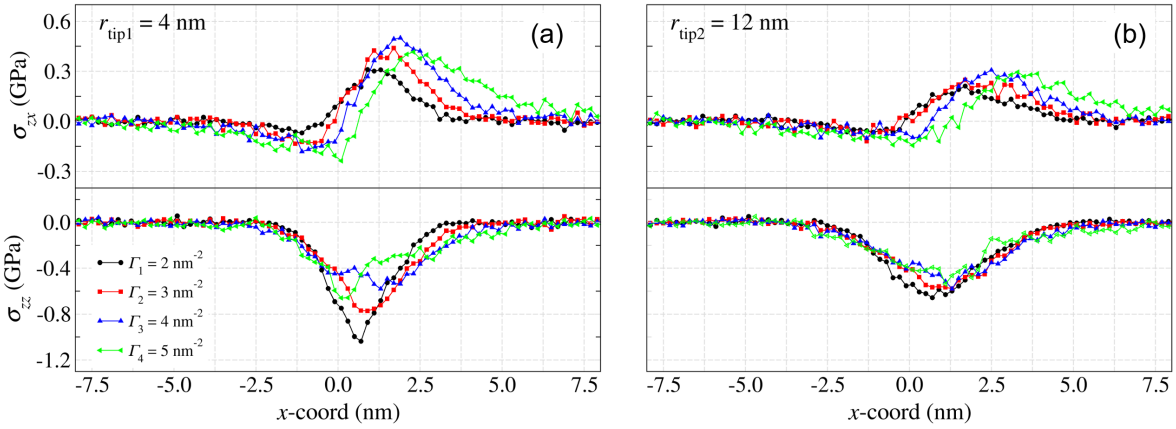

Figure 7: Spatial distribution (in the sliding direction) of shear stress, σ_{zx}, and normal stress, σ_{zz}, for tip radii, $r_{\mathrm{tip}} = 4$ nm (a) and 12 nm (b), at the highest load considered ($F_{\mathrm{N}} = 30$ nN).

Fig. 7 shows that σ_{zx} is mostly localised towards the leading edge of the tip. The same observation has been made previously in NEMD simulations of contacting solid nanoasperities[89] as well as close-packed alkyl monolayers indented with a spherical fullerene tip.[46,84] In general, OFM atoms at the leading edge resist tip motion (positive σ_{zx}), while atoms at the trailing edge assist tip motion (negative σ_{zx}). This asymmetry is more prevalent at high coverage ($\Gamma = 4$–5 nm^{-2}). For the sharper tip (Fig. 7a), the σ_{zx} peaks are higher and more strongly localised than for the blunter tip (Fig. 7b). In Fig. 7a, σ_{zx} decays to zero within

3 nm of the centre of the tip at low coverage (Γ = 2 nm^{-2}), while it extends to over 8 nm at high coverage (Γ = 5 nm^{-2}). This suggests that molecular deformation extends much further in front of the leading edge of the tip at high coverage, suggesting slower relaxation due to the higher molecular density. The peak σ_{zx} is lower for Γ = 2 nm^{-2} and similar for Γ = 3–5 nm^{-2}. Looking at Fig. 5a, μ is lowest for Γ = 2 nm^{-2}, similar for Γ = 3 nm^{-2} and 5 nm^{-2}, and highest for 4 nm^{-2}. The increase in μ between Γ = 2–4 nm^{-2} can be attributed to the larger peak σ_{zx}, as well as a broader distribution of σ_{zx} in the sliding direction. The reduction in μ between Γ = 4–5 nm^{-2} is due to lower peak σ_{zx}, as well as negative σ_{zx} at the trailing edge indicating pushing forces from these molecules.

For most of the systems and conditions considered, the σ_{zz} distribution is Hertz-like. As expected, σ_{zz} is more strongly localised for the smaller tip, indicating higher local pressures. The maximum σ_{zz} is not localised directly underneath the center of the sliding tip, but rather towards the leading edge. Similar behaviour has also been observed in previous NEMD simulations of close-packed alkyl monolayers indented with a spherical fullerene tip.[46] For the sharp tip (r_{tip} = 4 nm) at low coverage (Γ = 2 nm^{-2}), the σ_{zz} peak located close to the centre of the tip is much sharper than for the other cases. Similar behaviour has previously been observed for compression simulations of contacting solid nanoasperities[54] as well as amorphous silica nanoasperities protected by low coverage OTS monolayers.[44,45] Strong localisation of σ_{zz} is indicative of larger local pressures than would be predicted using continuum contact mechanics models.[54] Since this only occurs for the sharpest tip, lowest coverage, and highest load considered, Hertz theory provides a reasonable approximation of the pressure distribution in these systems.

Morphology and Dissipation

To explore connections between the monolayer morphology and friction, we also investigated changes in molecular orientation and thermal dissipation during sliding. For this purpose, mean positions of coarsened tailgroup carbon atoms projected in the xz plane ($\boldsymbol{r}_{\mathrm{mean}}$) and

their radii of gyration (R_g) were calculated. Fig. 8 shows a representative case where r_{tip} = 4 nm and F_N = 30 nN.

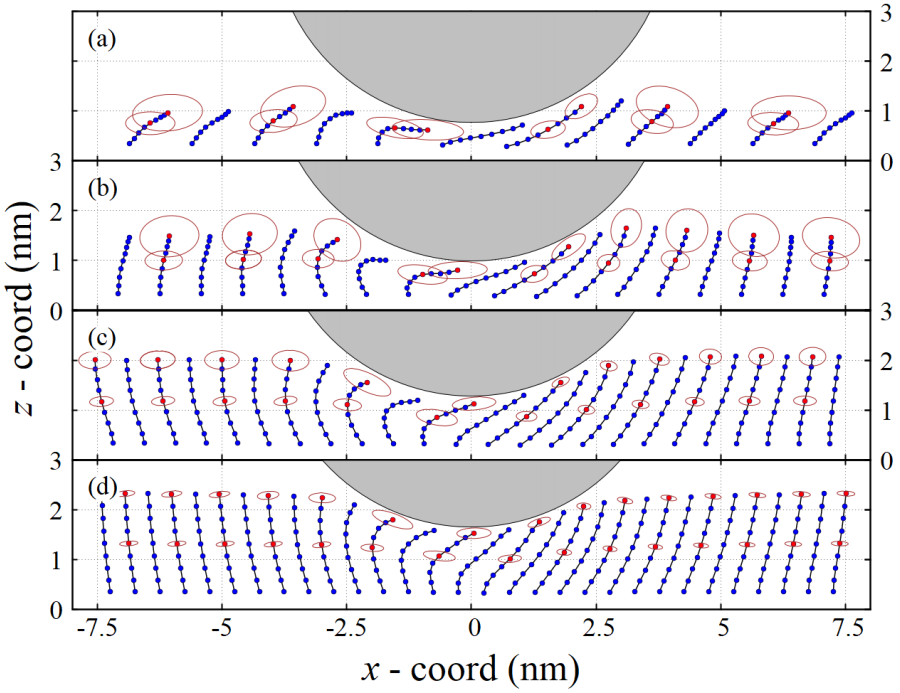

Figure 8: Coarsened molecular morphology of the OFM monolayers during sliding in the case of r_{tip} = 4 nm, F_N = 30 nN. Blue circles represent the mean positions of the tailgroup carbons projected in the xz plane and ellipses represent radius of gyration of the central and terminal (in red) tailgroup atoms. Bin size, Δx = 1.25, 0.833, 0.625, 0.5 nm for Γ = 2, 3, 4, 5 nm^{-2}, respectively.

Each blue circle in Fig. 8 represents the spatially-resolved position of the i^{th} tailgroup carbon in a coarsened molecule j over the observation time τ_{obs}. The bin size, Δx, varies depending on Γ such that each coarsened molecules represents a projection of the conformation of the stearamide tailgroups in the xz plane. For this purpose, Δx = 1.25, 0.833, 0.625, 0.5 nm for Γ = 2, 3, 4, 5 nm^{-2}, respectively. The molecule index is determined only by the coordination of carbon i=1 (the anchoring site), while the rest of the carbons are automatically associated with the same bin. Since there is only one coarsened molecule in each bin, the bin index is equal to the coarsened molecule index. The radius of gyration of each coarsened carbon is calculated via $R_g^i = < \frac{1}{N_j} \sum_1^{N_j} (\boldsymbol{r}_j^i - \boldsymbol{r}_{mean}^i)^{1/2} >$, where $\boldsymbol{r}_j^i$ denotes

the position of the i^{th} carbon in a sample molecule, N_j the total number of sample molecules in bin j, and <> represents an ensemble average. Each R_{g} is shown as an ellipse for the corresponding mean position (highlighted in red) with its radii representing $R_{\text{g},x}$ and $R_{\text{g},z}$, respectively. Here, $R_{\text{g},x}$ and $R_{\text{g},z}$ are in the principal axis. To enable clearer visualization, only $\boldsymbol{r}_{\text{mean}}$ with carbon index of $i = 2n$ (n = 1,...,9) are shown; and for the same reason, R_{g} is also shown selectively.

Fig. 8 shows that the stearamide molecules become more upright, more extended (more separated $\boldsymbol{r}_{\text{mean}}$), and less mobile (smaller R_{g}) as Γ increases. These observations are in agreement with previous NEMD simulations[37] as well as QCM and ellipsometry experiments of a range of OFMs adsorbed on oxide surfaces.[17] At low Γ, the stearamide molecules adopt a flatter conformation to maximise van der Waals interactions between the tailgroups and the surfaces, as shown in previous DFT calculations.[51] At high Γ, van der Waals interactions between proximal tailgroups lead the molecules to adopt an upright, $all{-}trans$ conformation, and only molecules directly underneath the tip contain gauche defects. In general, molecules located at the leading edge of the tip are deformed in the direction of sliding and stretched, while those at the trailing edge bend forward and form gauche defects around halfway up the tailgroup. Localised gauche defects at the trailing edge of the sliding tip were also observed in previous NEMD simulations of OTS SAMs.[48]

Fig. 8 shows the change in the configuration of the coarsened molecules as the tip moves forward ($+x$) by a unit spacing of Δx = bin size. Thus, the conformation of molecule j changes to that of molecule j-1 (molecule j-1 located on the left hand side of molecule j in Fig. 8) after a time interval, $\Delta\tau = \Delta x/v_x$. In that sense, Fig. 8 depicts a dynamic evolution of the film in response to the sliding tip, with each molecule in a nonequilibrium steady state. By comparing the configurations of a molecule at τ and $\tau{+}\Delta\tau$, one can measure the deviation of its position from a previous time frame: $\Delta\boldsymbol{r}(\Delta\tau) = \boldsymbol{r}_{j-1} - \boldsymbol{r}_j + \Delta x$. The location dependence of the molecular instability can be evaluated in terms of a temperature rise (ΔT = T-T_0) by assuming that $T \propto \boldsymbol{v}^2$, where $\boldsymbol{v} = \Delta\boldsymbol{r}/\Delta\tau$. More specifically, T is derived from

$1/2\ m\ v_{xz}^2 = 1/2\ D_{dim}\ k_B\ T$, where m is the sum of the masses of the coarse-grained atoms in each bin, v_{xz} is the velocity in the xz plane, $D_{dim} = 2$, k_B is Boltzmann's constant. T_0 is the simulation temperature, 300 K. Note, the purpose here is not to quantitatively determine the instantaneous temperature rise, but rather to show differences in thermal dissipation between the different monolayer coverages. This should help to demonstrate the connection between tip-induced changes in molecular morphology with dynamic instabilities within the molecules.

Fig. 9 shows a normalised percentage $\Delta T/T_0$ mapping for the aforementioned representative case. The mean positions of the coarsened carbon atoms are shown to relate the dissipation and changes to the conformation of the stearamide molecules. In the case of Γ = 2 nm^{-2}, ΔT is very small and is evenly distributed over the tip-monolayer contact area. When $\Gamma > 2$ nm^{-2}, ΔT becomes significant, and is localised predominantly towards the trailing edge of the tip. While ΔT becomes more localised as coverage increases, the magnitude of ΔT is greatest for the system with highest μ in Fig. 5 ($\Gamma = 4$ nm^{-2}). In all cases, ΔT is negligible at the molecule-surface interface due to efficient thermostatting. Looking at the coarsened atom positions in Fig. 9, the largest ΔT values correspond to where the molecules are most deformed from their undisturbed conformations. There is a strong propensity for those molecules to restore to their relaxed configurations and release the accumulated energy, particularly at high coverage ($\Gamma = 5$ nm^{-2}). This process is energetically beneficial and helps to reduce the friction forces as the molecules at the trailing edge push the tip forwards to recover their $all - trans$ conformations. This is evidenced by the negative forces at the trailing edge of the tip in Fig. 7, which have also been noted in previous NEMD studies.[46,84] This thermal dissipation is rather different to that observed in NEMD simulations of tips indenting solid surfaces, where the temperature rise localised at the leading edge of the tip in the pileup region.[77]

Fig. 6 showed a very weak, quasi-logarithmic dependence of friction on sliding velocity, which is consistent with Coulomb's friction law.[90] In order for such a dependence to be

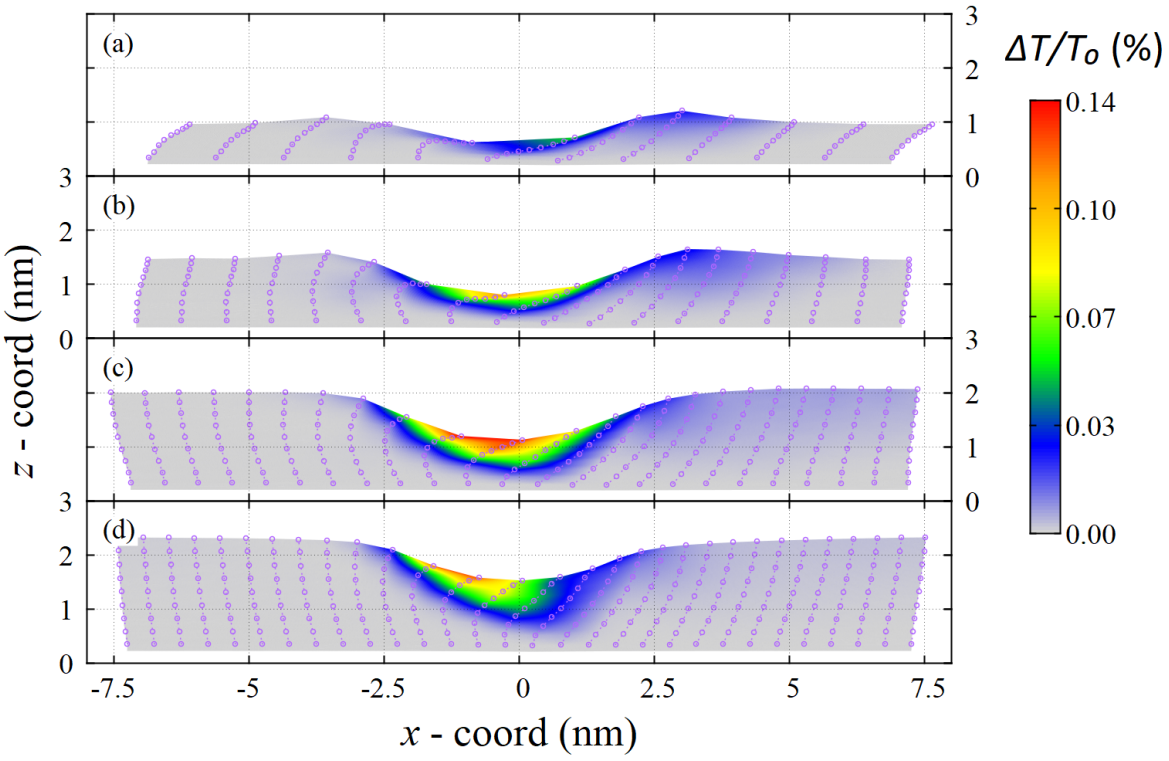

Figure 9: Mapping of the normalised percentage temperature rise ($\Delta T/T_0$) due to dynamic instability in the case of $r_{\text{tip}} = 4$ nm, $F_{\text{N}} = 30$ nN. Purple circles represent mean positions of tailgroup carbons projected in the xz plane.

obtained in a single-asperity contact, a system must undergo elastic or plastic instabilities, as rationalized in the Prandtl model.[91] During an instability, the stable position of an atom suddenly disappears in response to the relative (sliding) motion of two (solid) bodies and the atom quickly moves downward to the next minimum. In this process, potential energy is lost, the amount of which depends in leading order on the slid distance rather than on the sliding velocity. Such a process implies hysteresis, since the atom would not quickly revert to its previous metastable site if the sliding direction were instantaneously reversed. While Prandtl envisioned primarily non-linear elastic hysteresis in models of isolated atoms, the concept of instabilities leading to Coulomb-type friction extends to many different processes.[90] In fact, Prandtl rightfully claimed that his model can be used to describe the transition from Stokes to Coulomb friction, including the shear thinning of liquids.[92]

In the context of SAMs, the nature of sliding-induced instabilities is surprisingly little investigated. Most NEMD studies consider two perfectly flat surfaces in sliding motion,[36,37] in which case viscoelastic deformation arising due to asperity collision or plowing of a tip through a viscoelastic layer do not occur. These, however, were identified to be the predominant source of dissipation in asperity collisions of polymer brushes grafted to surfaces with nanoscale curvature.[85] Since the latter study was based on coarse-grained force fields, no typical molecular instabilities could occur, and thus no Coulomb friction regime was identified. Elucidating Coulomb friction mechanisms thus entails identification of potential molecular instabilities. Towards this end, the positions of coarse-grained atoms were averaged in the x-direction within the frame of reference of the moving tip, as shown in Fig. 8. This reveals that coarsened molecules are bent into a curved shape at the leading edge in a quasi-continuous fashion, which is where large frictional stresses act on the tip, as evidenced in Fig. 7. At the trailing edge, deformed molecules snap back to their elongated $all-trans$ conformation.

It could be argued that the temperature rise (Fig. 9) associated with these snaps is small, since the energies associated with the instabilities is < 1 % of the thermal energy.

However, direct comparisons may not be meaningful here for the following reasons. First, kinetic energy is measured at instantaneous times, while the positions of the coarse-grained atoms, and thus their velocities, are accrued over a 10 ps time scale. Second, the coarse-grained atoms move through a highly dissipate viscoelastic medium. Therefore, velocities corresponding to 1 % of the thermal velocities can be considered as very large. The coarse-grained velocities might therefore be better compared to the root-mean-square distances traveled by the coarse-grained atoms within the same time span. However, this depends on the relative position of a coarse-grained atom in a molecule and to the tip, so we decided to report the energy density increases relative to the thermal energies.

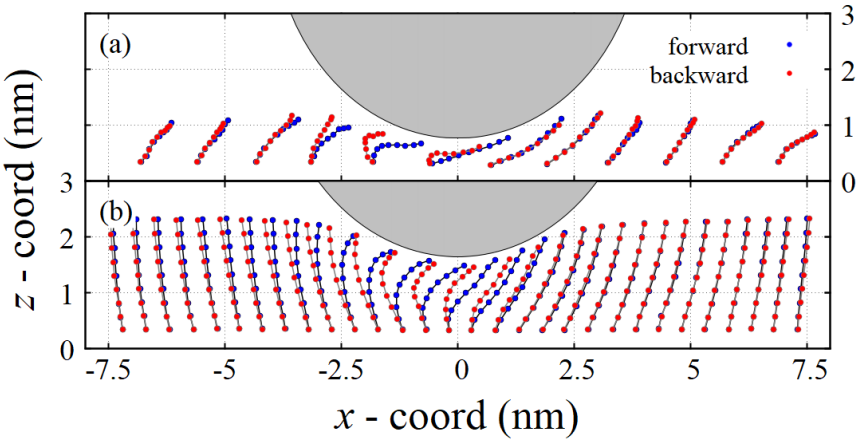

Figure 10: Coarsened molecular configuration from forward (blue) and backward (red) sliding in the cases of (a) $\Gamma = 2$ nm^{-2} and (b) $\Gamma = 5$ nm^{-2}, $r_{\text{tip}} = 4$ nm, $F_{\text{N}} = 30$ nN.

To substantiate our claim that the instabilities occur at the trailing edge of the moving tip, a sequence of simulations were conducted in which the tip was stopped and relaxed for 10 picoseconds. The tip velocity was then reverted for a distance whose linear dimension equaled the bin size over which the atom configurations were shown in Fig. 8. The results, shown in Fig. 10, indicate that while coarsened molecule positions are recovered at the leading edge following velocity reversal, this is not the case for molecules at the trailing edge. This clearly reveals structural hysteresis of the molecules at the trailing edge of the tip.

In simple model systems lubricated by atomic fluids,[89] it was also found that friction forces were localised at the leading edge of the tip; however, no pushing forces were observed at the trailing edge. Likewise, various systems show dissipation to take place at other locations than where friction forces are transmitted between two solids. For example, when intergranular sliding within a body is induced by a tribological interface, a significant amount of energy can be dissipated at those grain boundaries.[93] Similarly, rubber friction is thought to be caused to a significant degree by bulk viscoelastic deformation.[94] Generally speaking, the excitation of a surface mode of wavelength, λ, in regular viscoelasticity leads to a dissipative zone having a depth of roughly $\lambda/(2\pi)$. In our case, the dissipation takes place near the interface, but not directly in the region where the frictional forces act.

Conclusions

We have performed NEMD simulations using an all-atom force field to study frictional dissipation within OFM monolayers indented by sharp AFM tips. A wide range of surface coverages, tip radii, loads, sliding velocities were studied for stearamide monolayers, on an α-Fe_2O_3 substrate, indented by an a-SiO_2 tip. For all the systems and conditions considered, there is measurable tip-monolayer indentation, and friction is dominated by molecular plowing. Even stearamide monolayers with low surface coverage are able to mitigate direct solid-solid contact and withstand GPa-level local pressures applied by sharp tips and large loads. Friction forces increase linearly with normal force with finite intercepts, which can be adequately represented using the extension to Amonton's friction law as proposed by Derjaguin. Sharper tips give larger friction coefficients (due to deeper indentation), but smaller Derjaguin offsets (due to smaller contact area). A Coulomb-like relationship between friction and sliding velocity is observed, suggesting an instability during sliding. Indeed, we show that while normal and shear stresses are localised at the leading edge of the tip, thermal dissipation occurs mostly at the trailing edge. More specifically, the sliding tip deforms the

adsorbed molecules at its leading edge which snap back to relaxed conformations at the trailing edge.

We have uncovered the physical mechanisms driving the opposing friction-coverage relationships in nanoscale and macroscale experiments of OFMs. In macroscale tribology experiments, and previous NEMD simulations with flat surfaces, friction decreases with increasing OFM surface coverage since this leads more solid-like monolayers and reduced interdigitation. For the current NEMD simulations with sharp nanoscale asperities, which penetrate significantly into the OFM monolayers, non-monotonic friction-coverage behaviour is observed, which is due to a non-monotonic relationship between indentation depth and surface coverage. This is attributed to two competing effects of decreasing confinement-induced viscosity enhancement and increasing headgroup packing density as the OFM surface coverage is increased. Previous AFM experiments have either observed a decrease (for blunt tips) or increase (for sharp tips) in friction with increasing coverage. However, in future AFM experiments using sharp tips and OFMs which are known to form close-packed monolayer films, we expect non-monotonic friction-coverage to be observed.

Acknowledgement

H.G. thanks the Alexander von Humboldt Foundation for a Humboldt Research Fellowship. J.P.E. and D.D. thank the Engineering and Physical Sciences Research Council (EPSRC) for an Established Career Fellowship EP/N025954/1 and grant EP/P030211/1. We thank Carlos Ayestarán Latorre for useful discussions. All data reported in the manuscript can be obtained by emailing the corresponding author or tribology@imperial.ac.uk.

References

(1) Cheng, H. F.; Hu, Y. A. Influence of chain ordering on frictional properties of self-assembled monolayers (SAMs) in nano-lubrication. *Adv. Colloid Interface Sci.* **2012**,

171, 53–65.

(2) Zhu, Y.; Free, M. L.; Woollam, R.; Durnie, W. A review of surfactants as corrosion inhibitors and associated modeling. *Prog. Mater. Sci.* **2017**, *90*, 159–223.

(3) Heinz, H.; Pramanik, C.; Heinz, O.; Ding, Y.; Mishra, R. K.; Marchon, D.; Flatt, R. J.; Estrela-Lopis, I.; Llop, J.; Moya, S.; Ziolo, R. F. Nanoparticle decoration with surfactants: Molecular interactions, assembly, and applications. *Surf. Sci. Rep.* **2017**, *72*, 1–58.

(4) Spikes, H. Friction Modifier Additives. *Tribol. Lett.* **2015**, *60*, 5.

(5) Taylor, R. I. Tribology and energy efficiency: from molecules to lubricated contacts to complete machines. *Faraday Discuss.* **2012**, *156*, 361–382.

(6) Hardy, W. B.; Doubleday, I. Boundary lubrication - The paraffin series. *Proc. R. Soc. London, Ser. A* **1922**, *100*, 550–557.

(7) Bowden, F.; Leben, L. The Friction of Lubricated Metals. *Philos. Trans. R. Soc. London, Ser. A* **1940**, *239*, 1–27.

(8) Blodgett, K. B. Films Built by Depositing Successive Monomolecular Layers on a Solid Surface. *J. Am. Chem. Soc.* **1935**, *57*, 1007–1022.

(9) Ulman, A. Formation and structure of self-assembled monolayers. *Chem. Rev.* **1996**, *96*, 1533–1554.

(10) Spikes, H. A.; Cameron, A. A comparison of adsorption and boundary lubricant failure. *Proc. Roy. Soc. Lond. A.* **1974**, *336*, 407–419.

(11) Jahanmir, S.; Beltzer, M. An adsorption model for friction in boundary lubrication. *ASLE Trans.* **1986**, *29*, 423–430.

(12) Jahanmir, S.; Beltzer, M. Effect of Additive Molecular-Structure on Friction Coefficient and Adsorption. *J. Tribol.* **1986**, *108*, 109–116.

(13) Jaishankar, A.; Jusufi, A.; Vreeland, J. L.; Deighton, P.; Pellettiere, J. R.; Schilowitz, A. M. Adsorption of stearic acid at the iron oxide/oil interface - theory, experiments and modeling. *Langmuir* **2019**, *35*, 2033–2046.

(14) Spikes, H. A. Direct Observation of Boundary Layers. *Langmuir* **1996**, *12*, 4567–4573.

(15) Lundgren, S. M.; Persson, K.; Mueller, G.; Kronberg, B.; Clarke, J.; Chtaib, M.; Claesson, P. M. Unsaturated fatty acids in alkane solution: adsorption to steel surfaces. *Langmuir* **2007**, *23*, 10598–10602.

(16) Nalam, P. C.; Pham, A.; Castillo, R. V.; Espinosa-Marzal, R. M. Adsorption Behavior and Nanotribology of Amine-Based Friction Modifiers on Steel Surfaces. *J. Phys. Chem. C* **2019**, *123*, 13672–13680.

(17) Fry, B. M.; Moody, G.; Spikes, H. A.; Wong, J. S. S. Adsorption of Organic Friction Modifier Additives. *Langmuir* **2020**, *36*, 1147–1155.

(18) Wood, M. H.; Welbourn, R. J. L.; Charlton, T.; Zarbakhsh, A.; Casford, M. T.; Clarke, S. M. Hexadecylamine Adsorption at the Iron Oxide-Oil Interface. *Langmuir* **2013**, *29*, 13735–13742.

(19) Wood, M. H.; Casford, M. T.; Steitz, R.; Zarbakhsh, A.; Welbourn, R. J. L.; Clarke, S. M. Comparative Adsorption of Saturated and Unsaturated Fatty Acids at the Iron Oxide/Oil Interface. *Langmuir* **2016**, *32*, 534.

(20) Szlufarska, I.; Chandross, M.; Carpick, R. W. Recent advances in single-asperity nanotribology. *J. Phys. D: Appl. Phys.* **2008**, *41*, 123001.

(21) Simič, R.; Kalin, M. Adsorption mechanisms for fatty acids on DLC and steel studied by AFM and tribological experiments. *Appl. Surf. Sci.* **2013**, *283*, 460–470.

(22) Campen, S.; Green, J. H.; Lamb, G. D.; Spikes, H. A. In Situ Study of Model Organic Friction Modifiers Using Liquid Cell AFM: Self-Assembly of Octadecylamine. *Tribol. Lett.* **2015**, *58*, 39.

(23) Campen, S.; Green, J. H.; Lamb, G. D.; Spikes, H. A. In Situ Study of Model Organic Friction Modifiers Using Liquid Cell AFM; Saturated and Mono-unsaturated Carboxylic Acids. *Tribol. Lett.* **2015**, *57*, 18.

(24) Ruths, M.; Lundgren, S.; Danerlov, K.; Persson, K. Friction of fatty acids in nanometer-sized contacts of different adhesive strength. *Langmuir* **2008**, *24*, 1509–1516.

(25) Xiao, X.; Hu, J.; Charych, D. H.; Salmeron, M. Chain Length Dependence of the Frictional Properties of Alkylsilane Molecules Self-Assembled on Mica Studied by Atomic Force Microscopy. *Langmuir* **1996**, *12*, 235–237.

(26) Lio, A.; Charych, D. H.; Salmeron, M. Comparative atomic force microscopy study of the chain length dependence of frictional properties of alkanethiols on gold and alkylsilanes on Mica. *J. Phys. Chem. B* **1997**, *101*, 3800–3805.

(27) McDermott, M. T.; Green, J.-B. D.; Porter, M. D. Scanning Force Microscopic Exploration of the Lubrication Capabilities of n-Alkanethiolate Monolayers Chemisorbed at Gold: Structural Basis of Microscopic Friction and Wear. *Langmuir* **1997**, *13*, 2504–2510.

(28) Lee, S.; Shon, Y.-S.; Colorado, R.; Guenard, R. L.; Lee, T. R.; Perry, S. S. The Influence of Packing Densities and Surface Order on the Frictional Properties of Alkanethiol Self-Assembled Monolayers (SAMs) on Gold: A Comparison of SAMs Derived from Normal and Spiroalkanedithiols. *Langmuir* **2000**, *16*, 2220–2224.

(29) Shon, Y. S.; Lee, S.; Colorado, R.; Perry, S. S.; Lee, T. R. Spiroalkanedithiol-based SAMs reveal unique insight into the wettabilities and frictional properties of organic thin films. *J. Am. Chem. Soc.* **2000**, *122*, 7556–7563.

(30) Foster, T. T.; Alexander, M. R.; Leggett, G. J.; McAlpine, E. Friction force microscopy of alkylphosphonic acid and carboxylic acids adsorbed on the native oxide of aluminum. *Langmuir* **2006**, *22*, 9254–9259.

(31) Brukman, M. J.; Marco, G. O.; Dunbar, T. D.; Boardman, L. D.; Carpick, R. W. Nanotribological Properties of Alkanephosphonic Acid Self-Assembled Monolayers on Aluminum Oxide: Effects of Fluorination and Substrate Crystallinity. *Langmuir* **2006**, *22*, 3988–3998.

(32) Flater, E. E.; Ashurst, W. R.; Carpick, R. W. Nanotribology of octadecyltrichlorosilane monolayers and silicon: Self-mated versus unmated interfaces and local packing density effects. *Langmuir* **2007**, *23*, 9242–9252.

(33) Yang, Y.; Ruths, M. Friction of Polyaromatic Thiol Monolayers in Adhesive and Non-adhesive Contacts. *Langmuir* **2009**, *1894*, 12151–12159.

(34) Yang, Y.; Singh, J.; Ruths, M. Friction of aromatic thiol monolayers on silver: SFA and AFM studies of adhesive and non-adhesive. *RSC Adv.* **2014**, *4*, 18801–18810.

(35) Ewen, J. P.; Heyes, D. M.; Dini, D. Advances in nonequilibrium molecular dynamics simulations of lubricants and additives. *Friction* **2018**, *6*, 349–386.

(36) Doig, M.; Warrens, C. P.; Camp, P. J. Structure and friction of stearic acid and oleic acid films adsorbed on iron oxide surfaces in squalane. *Langmuir* **2014**, *30*, 186–195.

(37) Ewen, J. P.; Gattinoni, C.; Morgan, N.; Spikes, H. A.; Dini, D. Nonequilibrium Molecular Dynamics Simulations of Organic Friction Modifiers Adsorbed on Iron Oxide Surfaces. *Langmuir* **2016**, *32*, 4450.

(38) Eder, S. J.; Vernes, A.; Betz, G. On the Derjaguin Offset in Boundary-Lubricated Nanotribological Systems. *Langmuir* **2013**, *29*, 13760–13772.

(39) Ewen, J. P.; Echeverri Restrepo, S.; Morgan, N.; Dini, D. Nonequilibrium molecular dynamics simulations of stearic acid adsorbed on iron surfaces with nanoscale roughness. *Tribol. Int.* **2017**, *107*, 264–273.

(40) Campen, S.; Green, J.; Lamb, G.; Atkinson, D.; Spikes, H. On the increase in boundary friction with sliding speed. *Tribol. Lett.* **2012**, *48*, 237–248.

(41) Tutein, A. B.; Stuart, S. J.; Harrison, J. A. Indentation Analysis of Linear-Chain Hydrocarbon Monolayers Anchored to Diamond. *J. Phys. Chem. B* **1999**, *22*, 11357–11365.

(42) Salmeron, M. Generation of defects in model lubricant monolayers and their contribution to energy dissipation in friction. *Tribol. Lett.* **2001**, *10*, 69–79.

(43) Meltzer, C.; Paul, J.; Dietrich, H.; Ja, C. M.; Clark, T.; Zahn, D.; Peukert, W. Indentation and Self-Healing Mechanisms of a Self-Assembled Monolayer - A Combined Experimental and Modeling Study. *J. Am. Chem. Soc.* **2014**, *136*, 10718–10727.

(44) Ewers, B. W.; Batteas, J. D. The role of substrate interactions in the modification of surface forces by self-assembled monolayers. *RSC Adv.* **2014**, *4*, 16803–16812.

(45) Ewers, B. W.; Batteas, J. D. Utilizing Atomistic Simulations To Map Pressure Distributions and Contact Areas in Molecular Adlayers within Nanoscale Surface-Asperity Junctions: A Demonstration with Octadecylsilane-Functionalized Silica Interfaces. *Langmuir* **2014**, *30*, 11897–11905.

(46) Knippenberg, M. T.; Mikulski, P. T.; Dunlap, B. I.; Harrison, J. A. Atomic contributions to friction and load for tip-self-assembled monolayers interactions. *Phys. Rev. B* **2008**, *78*, 235409.

(47) Chandross, M.; Lorenz, C. D.; Stevens, M. J.; Grest, G. S. Simulations of nanotribology with realistic probe tip models. *Langmuir* **2008**, *24*, 1240–1246.

(48) Summers, A. Z.; Iacovella, C. R.; Cummings, P. T.; McCabe, C. Investigating Alkylsilane Monolayer Tribology at a Single-Asperity Contact with Molecular Dynamics Simulation. *Langmuir* **2017**, *33*, 11270–11280.

(49) Jorgensen, W. L.; Maxwell, D. S.; Tirado-Rives, J. Development and testing of the OPLS all-atom force field on conformational energetics and properties of organic liquids. *J. Am. Chem. Soc.* **1996**, *118*, 11225–11236.

(50) Siu, S. W. I.; Pluhackova, K.; Bockmann, R. A. Optimization of the OPLS-AA Force Field for Long Hydrocarbons. *J. Chem. Theory Comput.* **2012**, *8*, 1459–1470.

(51) Gattinoni, C.; Ewen, J. P.; Dini, D. Adsorption of Surfactants on α-Fe2O3(0001): A Density Functional Theory Study. *J. Phys. Chem. C* **2018**, *122*, 20817–20826.

(52) Ayestarán Latorre, C.; Ewen, J. P.; Gattinoni, C.; Dini, D. Simulating Surfactant-Iron Oxide Interfaces: From Density Functional Theory to Molecular Dynamics. *J. Phys. Chem. B* **2019**, *123*, 6870–6881.

(53) Raider, S. I.; Flitsch, R.; Aboaf, J. A.; Pliskin, W. A. Surface Oxidation of Silicon Nitride Films. *J. Electrochem. Soc.* **1976**, *123*, 560–565.

(54) Luan, B. Q.; Robbins, M. O. The breakdown of continuum models for mechanical contacts. *Nature* **2005**, *435*, 929–932.

(55) de Beer, S.; den Otter, W. K.; van den Ende, D.; Briels, W. J.; Mugele, F. Can confinement-induced variations in the viscous dissipation be measured? *Tribol. Lett.* **2012**, *48*, 1–9.

(56) Oh, S. J.; Cook, D. C.; Townsend, H. E. Characterization of iron oxides commonly formed as corrosion products on steel. *Hyperfine Interact.* **1998**, *112*, 59–66.

(57) Humphrey, W.; Dalke, A.; Schulten, K. VMD: Visual molecular dynamics. *J. Mol. Graph. Model.* **1996**, *14*, 33–38.

(58) Ingram, M.; Noles, J.; Watts, R.; Harris, S.; Spikes, H. A. Frictional Properties of Automatic Transmission Fluids: Part I-Measurement of Friction-Sliding Speed Behavior. *Tribol. Trans.* **2011**, *54*, 145–153.

(59) Briscoe, B. J.; Mustafaev, V.; Tabor, D. Lubrication of polythene by oleamide and stearamide. *Wear* **1972**, *19*, 399–414.

(60) Ramirez, M. X.; Hirt, D. E.; Wright, L. L. AFM Characterization of Surface Segregated Erucamide and Behenamide in Linear Low Density Polyethylene Film. *Nano Lett.* **2002**, *2*, 9–12.

(61) Ewen, J. P.; Gattinoni, C.; Thakkar, F. M.; Morgan, N.; Spikes, H.; Dini, D. A Comparison of Classical Force-Fields for Molecular Dynamics Simulations of Lubricants. *Materials.* **2016**, *9*, 651.

(62) Blake, R. L.; Hessevick, R. E.; Finger, L. W. Refinement of the Hematite Structure. *Am. Mineral.* **1966**, *51*, 123–129.

(63) Berro, H.; Fillot, N.; Vergne, P. Molecular dynamics simulation of surface energy and ZDDP effects on friction in nano-scale lubricated contacts. *Tribol. Int.* **2010**, *43*, 1811–1822.

(64) van Beest, B. W. H.; Kramer, G. J.; van Santen, R. A. Force Fields for Silicas and Aluminophosphates Based on Ab Initio Calculations. *Phys. Rev. Lett.* **1990**, *64*, 1955–1958.

(65) Dopke, M. F.; Lutzenkirchen, J.; Moultos, O. A.; Siboulet, B.; Dufreche, J.-F.; Padding, J. T.; Hartkamp, R. Preferential Adsorption in Mixed Electrolytes Confined by Charged Amorphous Silica. *J. Phys. Chem. C* **2019**, *123*, 16711–16720.

(66) Yeh, I. C.; Berkowitz, M. L. Ewald summation for systems with slab geometry. *J. Chem. Phys.* **1999**, *111*, 3155–3162.

(67) Plimpton, S. Fast Parallel Algorithms for Short-Range Molecular Dynamics. *J. Comput. Phys.* **1995**, *117*, 1 – 19.

(68) Schneider, T.; Stoll, E. Molecular-dynamics study of a three-dimensional one-component model for distortive phase-transitions. *Phys. Rev. B* **1978**, *17*, 1302–1322.

(69) Bernardi, S.; Todd, B. D.; Searles, D. J. Thermostating highly confined fluids. *J. Chem. Phys.* **2010**, *132*, 244706.

(70) Yong, X.; Zhang, L. T. Thermostats and thermostat strategies for molecular dynamics simulations of nanofluidics. *J. Chem. Phys.* **2013**, *138*, 084503.

(71) Sam, A.; Kannam, S. K.; Hartkamp, R.; Sathian, S. P. Water flow in carbon nanotubes: The effect of tube flexibility and thermostat. *J. Chem. Phys.* **2017**, *146*, 234701.

(72) Chandross, M.; Lorenz, C. D.; Grest, G. S.; Stevens, M. J.; Webb III, E. B. Nanotribology of Anti-Friction Coatings in MEMS. *JOM* **2005**, *57*, 55–61.

(73) Taylor, R. I.; de Kraker, B. R. Shear rates in engines and implications for lubricant design. *Proc. Inst. Mech. Eng. Part J.* **2017**, *231*, 1106–1116.

(74) Echeverri Restrepo, S.; van Eijk, M. C. P.; Ewen, J. P. Behaviour of n-alkanes confined between iron oxide surfaces at high pressure and shear rate: A nonequilibrium molecular dynamics study. *Tribol. Int.* **2019**, *137*, 420–432.

(75) Jabbarzadeh, A. Friction anisotropy and asymmetry in self assembled monolayers. *Tribol. Int.* **2016**, *102*, 600–607.

(76) Salmeron, M.; Neubauer, G.; Folch, A.; Tomitori, M.; Ogletree, D. F.; Sautet, P. Viscoelastic and Electrical Properties of Self-Assembled Monolayers on Au(111) Films. *Langmuir* **1993**, *9*, 3600–3611.

(77) Stephan, S.; Dyga, M.; Urbassek, H. M.; Hasse, H. The Influence of Lubrication and the Solid-Fluid Interaction on Thermodynamic Properties in a Nanoscopic Scratching Process. *Langmuir* **2019**, *35*, 16948–16960.

(78) Houston, J. E.; Kim, H. I. Adhesion, friction, and mechanical properties of functionalized alkanethiol self-assembled monolayers. *Acc. Chem. Res.* **2002**, *35*, 547–553.

(79) Gao, H.; Müser, M. H. Why liquids can appear to solidify during squeeze-out - even when they don't. *J. Colloid Interface Sci.* **2020**, *562*, 273–278.

(80) Granick, S. Motions and relaxations of confined liquids. *Science.* **1991**, *253*, 1374–1379.

(81) Derjaguin, B. Molekulartheorie der äuβeren Reibung. *Z. Phys. A* **1934**, *88*, 661–675.

(82) Briscoe, B. J.; Evans, D. C. B. The shear properties of Langmuir-Blodgett layers. *Proc. R. Soc. London, Ser. A* **1982**, *380*, 389–407.

(83) Brewer, N. J.; Beake, B. D.; Leggett, G. J. Friction force microscopy of self-assembled monolayers: Influence of adsorbate alkyl chain length, terminal group chemistry, and scan velocity. *Langmuir* **2001**, *17*, 1970–1974.

(84) Knippenberg, M. T.; Mikulski, P. T.; Harrison, J. A. Effects of tip geometry on interfacial contact forces. *Model. Simul. Mater. Sci. Eng.* **2010**, *18*, 034002.

(85) de Beer, S.; Müser, M. H. Alternative dissipation mechanisms and the effect of the solvent in friction between polymer brushes on rough surfaces. *Soft Matter* **2013**, *9*, 7234–7241.

(86) Bowden, F.; Tabor, D. Friction, lubrication and wear: a survey of work during the last decade. *Br. J. Appl. Phys.* **1966**, *17*, 1521–1544.

(87) Yoshizawa, H.; Chen, Y. L.; Israelachvili, J. Fundamental mechanisms of interfacial friction. 1. relation between adhesion and friction. *J. Phys. Chem.* **1993**, *97*, 4128–4140.

(88) Tsukruk, V. V.; Bliznyuk, V. N.; Hazel, J.; Visser, D.; Everson, M. P. Organic Molecular Films under Shear Forces: Fluid and Solid Langmuir Monolayers. *Langmuir* **1996**, *12*, 4840–4849.

(89) Wenning, L.; Müser, M. H. Friction laws for elastic nanoscale contacts. *Europhys. Lett.* **2001**, *54*, 693.

(90) Müser, M. H.; Urbakh, M.; Robbins, M. O. In *Adv. Chem. Phys.*; Prigogine, I., Rice, S. A., Eds.; Wiley, 2003; Vol. 126; Chapter 5, pp 187–272.

(91) Prandtl, L. Ein Gedankenmodell zur kinetischen Theorie der festen Körper. *Z. Angew. Math. Mech.* **1928**, *8*, 85–106.

(92) Müser, M. H. Shear Thinning in the Prandtl Model and Its Relation to Generalized Newtonian Fluids. *Lubricants* **2020**, *8*, 38.

(93) Ma, E. Instabilities and ductility of nanocrystalline and ultrafine-grained metals. *Scr. Mater.* **2003**, *49*, 663–668.

(94) Persson, B. N. J. Theory of rubber friction and contact mechanics. *J. Chem. Phys.* **2001**, *115*, 3840–3861.

Graphical TOC Entry